

## Modeling a short dc discharge with thermionic cathode and auxiliary anode

E. Bogdanov, V. I. Demidov, I. D. Kaganovich, M. E. Koepke, and A. A. Kudryavtsev

Citation: *Phys. Plasmas* **20**, 101605 (2013); doi: 10.1063/1.4823464

View online: <http://dx.doi.org/10.1063/1.4823464>

View Table of Contents: <http://pop.aip.org/resource/1/PHPAEN/v20/i10>

Published by the [AIP Publishing LLC](#).

---

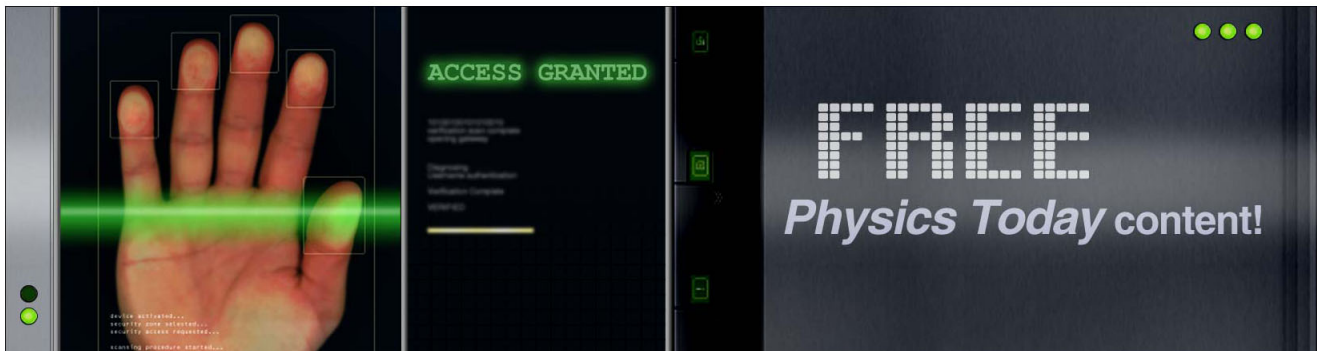
### Additional information on *Phys. Plasmas*

Journal Homepage: <http://pop.aip.org/>

Journal Information: [http://pop.aip.org/about/about\\_the\\_journal](http://pop.aip.org/about/about_the_journal)

Top downloads: [http://pop.aip.org/features/most\\_downloaded](http://pop.aip.org/features/most_downloaded)

Information for Authors: <http://pop.aip.org/authors>



## Modeling a short dc discharge with thermionic cathode and auxiliary anode

E. Bogdanov,<sup>1,2</sup> V. I. Demidov,<sup>1,3</sup> I. D. Kaganovich,<sup>4</sup> M. E. Koepke,<sup>3</sup> and A. A. Kudryavtsev<sup>1</sup>

<sup>1</sup>St. Petersburg State University, St. Petersburg 199034, Russia

<sup>2</sup>University ITMO, Kronverkskiy pr. 49, St. Petersburg 197101, Russia

<sup>3</sup>West Virginia University, Morgantown, West Virginia 26506, USA

<sup>4</sup>Princeton Plasma Physics Laboratory, Princeton, New Jersey 08543, USA

(Received 25 April 2013; accepted 12 July 2013; published online 10 October 2013)

A short dc discharge with a thermionic cathode can be used as a current and voltage stabilizer, but is subject to current oscillation. If instead of one anode two anodes are used, the current oscillations can be reduced. We have developed a kinetic model of such a discharge with two anodes, where the primary anode has a small opening for passing a fraction of the discharge current to an auxiliary anode. The model demonstrates that the current-voltage relationship of the discharge with two anodes is characterized everywhere by positive slope, i.e., positive differential resistance. Therefore, the discharge with two anodes is expected to be stable to the spontaneous oscillation in current that is induced by negative differential resistance. As a result, such a discharge can be used in an engineering application that requires stable plasma, such as a current and voltage stabilizer. © 2013 AIP Publishing LLC. [<http://dx.doi.org/10.1063/1.4823464>]

### I. INTRODUCTION

The development of a nonlocal approach to the kinetic theory of discharges is responsible for continuous progress in the field for more than a decade. This approach was originated and pioneered by Tsendin<sup>1-3</sup> who recently passed away, leaving numerous pupils, including the co-authors of this paper, to advance nonlocal plasma research. Explaining and utilizing cathode fall, negative glow, anode regions, and other phenomena associated with the basic discharge are possible with this nonlocal plasma approach. This approach improves attempts to clarify and predict the formation of a non-Maxwellian electron energy-distribution function (EEDF) in RF discharges and to describe correctly striations and streamers in a high-voltage discharge. This approach is being applied currently in plasma engineering research.

The conversion of a short-gap, dc discharge<sup>4-11</sup> that incorporates a thermionic cathode from inherently unstable to inherently stable<sup>4</sup> is modeled here by employing a nonlocal approach. We provide a kinetic model for the discharge. This practical application is one of the last ideas that the authors discussed with Tsendin. This paper is dedicated to him and his valuable insights, some of which influenced this paper in important ways.

The experimental demonstration of transforming negative differential resistance to positive differential resistance and thereby suppressing current and voltage oscillations of a short-gap dc discharge<sup>4</sup> is accomplished by placing the auxiliary anode beyond the primary anode with respect to the cathode. The auxiliary anode collects the passing fraction of the cathode current through a small hole in the primary anode.

### II. DESCRIPTION OF THE EXPERIMENTAL DEVICE AND KINETIC MODEL

A schematic of the device being modeled is shown in Fig. 1. The discharge takes place between a grounded, thermionic cathode and a positively biased primary,

ring-shaped anode. The cathode and primary anode are disks with outer radii of 5 mm and 15 mm, respectively. The primary anode has a circular 1-mm-radius hole in the center. The cathode-anode gap is 8 mm.

The auxiliary anode has radius of 15 mm and is placed beyond the primary anode to form parallel planes with the cathode and the primary anode. The anode-anode gap is adjustable from 1 mm to 50 mm in the experiment. We perform simulations only for the case of 1 mm in anode-anode gap. Cathode-anode-gap plasma is bounded by a conical-shell electrode electrically connected to the cathode. The left and right ends of the conical electrode have radii of 5 mm and 15 mm, respectively. No electric connection exists from the cathode to either anode.

In Fig. 2, the typical current-voltage experimental characteristics of the cathode-anode gap are presented. Curves 1 and 2 both correspond to the case of zero auxiliary-anode

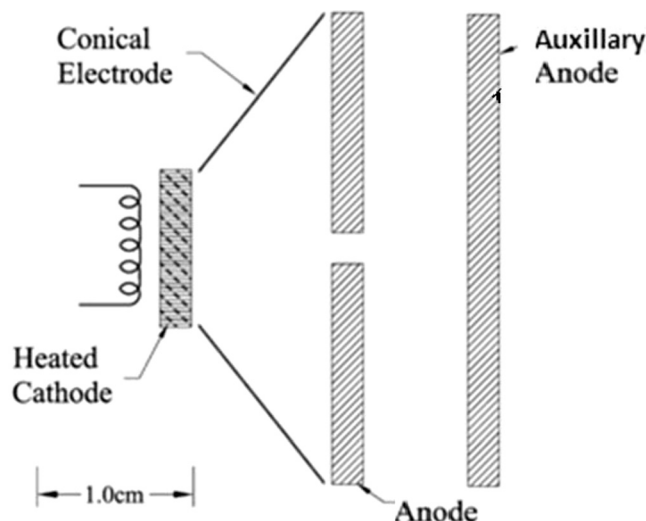


FIG. 1. A schematic diagram of the experimental device. The thermionic cathode is on the left, the primary anode is in the center, and the auxiliary anode is on the right.

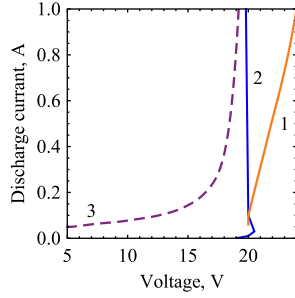


FIG. 2. Experimentally measured discharge current-voltage characteristic for helium gas pressure of (curve 1) 0.6 Torr and (curve 2) 1 Torr.<sup>4</sup> The thin current-free range of voltage values for the cathode-anode gap region is bounded by solid curves 1 and 2. The dashed curve corresponds to auxiliary current of 0.4 A and helium gas pressure of 1 Torr (3).<sup>4</sup>

current. It is evident from curve 1 in Fig. 2 that, in this voltage range and for pressure 0.6 Torr, the discharge has a positive discharge differential resistance. Increasing the gas pressure to 1 Torr or higher leads to the discharge differential resistance becoming slightly negative, thus causing spontaneous oscillations of the discharge voltage and current. Curve 3 corresponds to the case of fixed, nonzero, auxiliary-anode current. The emitted cathode current is the sum of the collected primary-anode current and the collected auxiliary-anode current. Observed, but not shown, is the trend that an increase in the auxiliary-anode current makes discharge differential resistance increasingly positive. In all cases with the positive differential resistance, the oscillations are practically absent and have negligible amplitude.

Two-dimensional modeling was performed in axially symmetric geometry where discharge dimensions in the model reproduced measured discharge dimensions. Background gas is helium at a pressure of 1 Torr. As shown in Ref. 12, under normal discharge conditions, the electron energy distribution function (EEDF) in the bulk plasma consists of two parts: low-energy, near-Maxwellian, plasma electrons with temperature of a few eV or lower and energetic-beam electrons emitted from the cathode and accelerated in the cathode sheath. For gas pressure of 1 Torr and discharge dimensions of 1 cm, the plasma-electron energy-relaxation length exceeds the cathode-anode gap. This means that the EEDF is a nonlocal function of electric field,<sup>1-3</sup> i.e., the EEDF is determined neither by the local values of the electric field nor by the plasma parameters at a given point. In the model presented in this paper, the low-energy plasma electrons are Maxwellian. Energetic electrons acquire energy in a cathode fall having magnitude approximately equal to the first excitation potential, and then undergo many elastic collisions. Therefore, their transport can be described by diffusion from cathode to anode and by losses due to inelastic collisions. After an energetic electron experiences an inelastic collision, its energy decreases to a low value and it becomes part of the Maxwellian plasma-electron population through electron-electron collisions. Correspondingly, we add these new low-energy electrons to the original bulk plasma electrons, taking into account energy conservation. Also, we consider only the regime of discharge when the plasma electric field and anode-hole-region electric field are weak and have negligible influence

on the energetic electrons. In the accompanying paper,<sup>13</sup> we studied another regime of the discharge where a potential drop appears in front of the anode hole (see details in Ref. 12). This potential drop accelerates and focuses energetic electrons into the hole. The model presented in this paper is limited and cannot describe that regime.

To summarize the model, the electron energy-distribution function consists of a Maxwellian plasma component and an energetic beam component having an energy determined by the cathode fall. This simplifying assumption justifies our use of the drift diffusion approximation for ion, energetic-beam electron, and low-energy plasma electron populations and use of the diffusion approximation for metastable atoms.

The system of balance equations for densities of the four types of particles, low-energy plasma electrons  $n_e$ , energetic electrons  $n_f$ , plasma ions  $n_i$ , and metastable helium atoms  $n_m$ , is expressed<sup>5</sup>

$$\nabla \cdot \Gamma_e = k_i n_e N_0 + k_{sw} n_e n_m + \tilde{k}_i n_f N_0 + \tilde{k}_{sw} n_f n_m, \quad (1)$$

$$\nabla \cdot \Gamma_i = k_i n_e N_0 + k_{sw} n_e n_m + \tilde{k}_i n_f N_0 + \tilde{k}_{sw} n_f n_m, \quad (2)$$

$$\nabla \cdot \Gamma_f = -(\tilde{k}_{exc} N_0 + \tilde{k}_i N_0 + \tilde{k}_{sw} n_m) \cdot n_f, \quad (3)$$

$$\nabla \cdot \Gamma_m = k_{exc} n_e N_0 + \tilde{k}_{exc} n_f N_0, \quad (4)$$

where  $\Gamma_j$  ( $j = e, i, f, m$ ) are the fluxes of corresponding particles,  $N_0$  is the density of the gas (helium) atoms, and  $k_{exc}$ ,  $k_i$ ,  $k_{sw}$  are the rate constants of excitation, direct ionization, and stepwise ionization by low-energy electrons, respectively. Corresponding rate constants of excitation, direct ionization, and stepwise ionization by energetic electrons are  $\tilde{k}_{exc}$ ,  $\tilde{k}_i$ , and  $\tilde{k}_{sw}$ . The fluxes of slow electrons and ions in drift-diffusion approximation are expressed<sup>5</sup>

$$\Gamma_e = -D_e \nabla n_e - \mu_e E n_e, \quad (5)$$

$$\Gamma_i = -D_i \nabla n_i + \mu_i E n_i, \quad (6)$$

where  $D_e$  and  $D_i$  are the diffusion coefficient of low-energy plasma electrons and plasma ions, respectively,  $\mu_e$  and  $\mu_i$  are their mobilities, and  $E$  is the electric field ( $E = -\nabla \phi$ , where  $\phi$  is the electrostatic potential). The flux of metastable helium atoms is determined by their diffusion, according to

$$\Gamma_m = -D_m \nabla n_m. \quad (7)$$

Energetic electrons acquire energy in the cathode fall. A weak electric field in the plasma and in the anode-hole region, where the potential drop is on the order the low-energy electron temperature, is assumed sufficiently small to have negligible influence on energetic electrons dynamics, which is dominated by free electron diffusion.<sup>14</sup> Thus, energetic electron flux is given by

$$\Gamma_f = -D_f \nabla n_f, \quad (8)$$

where  $D_f = v\lambda/3$  is the diffusion coefficient (here,  $v$  is the speed of the energetic electron and  $\lambda$  is the electron mean free path) depends on the local value of electric potential  $\phi$ .

At the cathode surface, i.e., at  $\varphi = 0$ , emitted electrons have nearly zero kinetic energy and subsequently become energetic after acceleration in the cathode sheath, i.e., the cathode fall. Thus, the local energetic-electron energy is  $w = e\varphi$  and

$$D_f = \frac{\sqrt{2e\varphi/m}}{3N_0 \cdot \sigma(e\varphi)}, \quad (9)$$

where  $\sigma$  is an energy-dependent cross-section of elastic scattering of electrons on atoms evaluated at the energy value equal to  $e\varphi$ . In Fig. 3 shows cross-sections of the processes with electrons in helium which have been used in this paper. Those cross-sections have been validated for plasma modeling in Ref. 21.

In the model,  $D_f$  was treated as a constant and  $w$  is equal to the local value of  $\varphi$ , which was spatially averaged over the central part of the discharge volume.

The electric potential was calculated by solving the Poisson equation

$$\nabla^2 \varphi = (n_e - n_i)/\epsilon_0, \quad (10)$$

where  $\epsilon_0$  is the permittivity of the vacuum. Note that for the investigated conditions in the plasma, the density of energetic electrons,  $n_f$  is small compared with the density of low-energy plasma electrons  $n_e$ , and, accordingly, the ambipolar electric field is determined by low-energy plasma electrons (see, e.g., Refs. 15 and 16)

$$E_a = -\frac{T_e \nabla n_e}{e n_e}. \quad (11)$$

The sheath potential drop near anode is determined by the current continuity equation. The primary anode collects both energetic-electron current and low-energy plasma-electron current. Note that varying the primary anode potential will change the collected plasma-electron current and will not change the energetic-electron current. Therefore, the

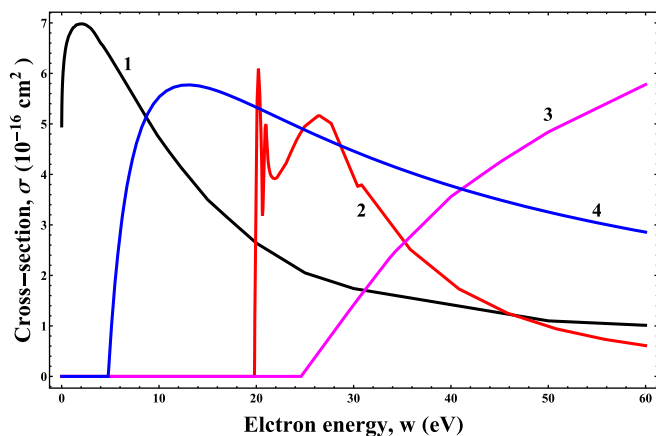


FIG. 3. The cross-sections of the processes with electrons in helium. The horizontal axis is the kinetic energy and the vertical axis is the cross-section. (1) Cross-section of elastic scattering (momentum transfer) of electrons, (2) metastable excitation cross section ( $\times 100$ ) for helium atoms, (3) direct ionization cross section ( $\times 20$ ) for helium atoms, and (4) stepwise ionization cross section from metastables.

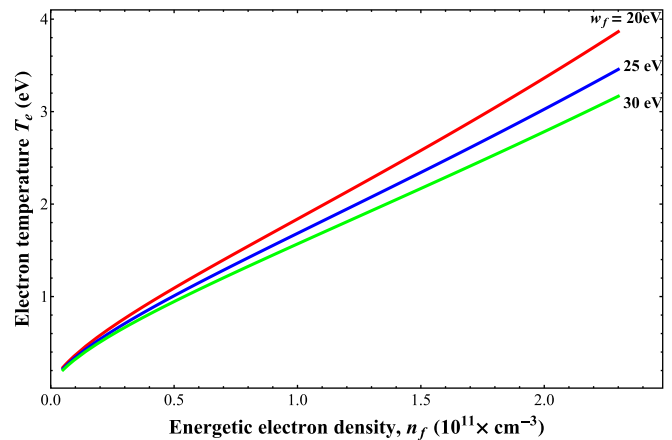


FIG. 4. The temperature of low-energy plasma electrons, calculated from Eq. (12) as a function of the density of energetic electrons for three different values of the energy of fast electrons: 20, 25, and 30 eV.

potential drop in the anode sheath depends on the densities of the plasma electrons and ions. For a given cathode-anode potential difference, the value of the cathode potential drop is uniquely related to the magnitude of the potential of the primary-anode sheath potential drop and the cathode fall.

As already mentioned, the model assumed the low-energy EEDF as a Maxwellian with a temperature of electrons  $T_e$  of few electron volts. The analysis shows that the energy balance of Maxwellian plasma electrons is mainly determined by heating due Coulomb collisions with energetic electrons and cooling due to energy losses in elastic collisions with atoms, so that their temperatures can be evaluated from the balance equation (see, e.g., Refs. 17 and 18)

$$\nu_{ee}(n_f)w_f = (T_e - T)\delta\nu_{ea}(T_e), \quad (12)$$

where  $\nu_{ee}(n_f)$  is the frequency of electron-electron collisions of energetic electrons with low-energy plasma electrons,  $\nu_{ea}(T_e)$  is the effective frequency of elastic collisions of low-energy plasma electrons with atoms,  $w_f$  is the energy of energetic electrons and  $T$  is the gas temperature, and  $\delta$  is the electron-to-atom-mass ratio. Figure 4 shows the temperature

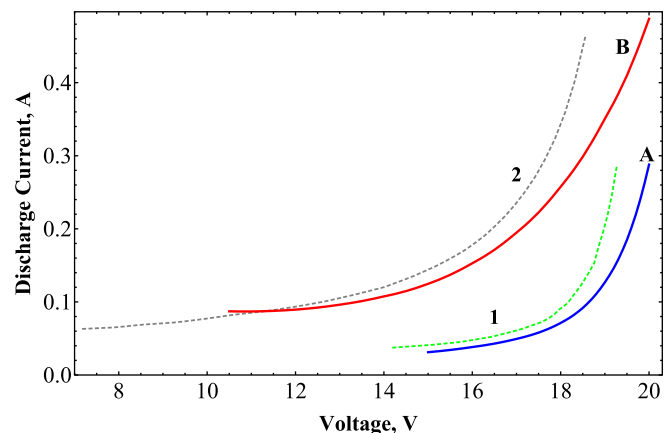


FIG. 5. The calculated current-voltage characteristics of the cathode-anode gap for auxiliary anode current of 0.2 A (A) and 0.4 A (B). Dashed lines are the corresponding experimental characteristics,<sup>19,20</sup> where curves 1 and 2 correspond to the anode currents of 0.2 and 0.4 A.

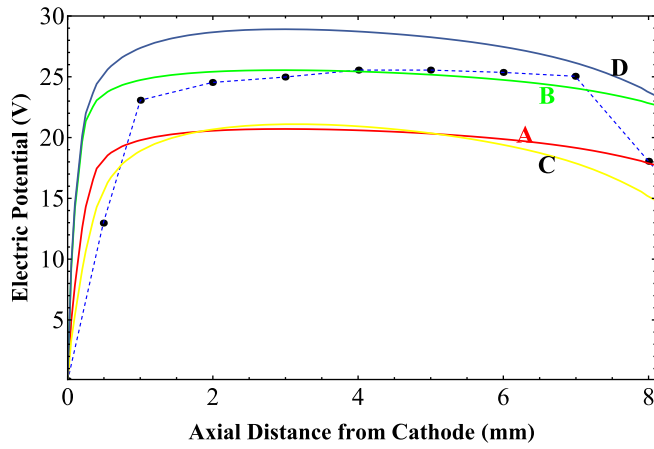


FIG. 6. Axial profile of potential. Curves A-D mark profiles associated with different operational modes. (A)  $T_e = 1$  eV,  $U_d = 15$  V; (B)  $T_e = 1$  eV,  $U_d = 19$  V; (C)  $T_e = 2$  eV,  $U_d = 10.5$  V; and (D)  $T_e = 2$  eV,  $U_d = 20$  V; Dots mark the experimentally measured potential profile for anode potential of 13 V.

dependence of low-energy plasma electrons, calculated from Eq. (12) as a function of the density of energetic electrons.

From Fig. 4, it is evident that  $T_e$  has a value of a few eV. Accordingly,  $\mu_e$  and the constants  $k_{exc}$ ,  $k_i$ , and  $k_{sw}$  have been calculated as convolutions of Maxwellian EEDF with the relevant cross-sections of the corresponding processes (see Fig. 3). Constants  $\bar{k}_{exc}$ ,  $\bar{k}_i$ , and  $\bar{k}_{sw}$ , including contributions from energetic electrons, were calculated by convoluting the corresponding cross-sections with the EEDF of energetic electrons

$$f_{0f}(X, W) = n_f(X) \frac{\delta(w - e\phi(X))}{\sqrt{e\phi(X)}}, \quad (13)$$

where  $\delta$  is the Dirac function. That is

$$\tilde{k}_j = \sqrt{2e/m} \cdot \sigma_j(e\phi) \cdot \sqrt{e\phi}, \quad (14)$$

where  $j$  has one of the following values, *exc*, *i*, and *sw*. The boundary conditions for the low-energy plasma electrons, plasma ions, and metastable helium atoms are similar, that

is, the normal component of the flow is equal to  $nV_{th}/4$ , where  $n$  is appropriate value of density near the border and  $V_{th}$  is the respective thermal speed for each species. For energetic electrons, we adopt the value of current at the cathode as a fitting parameter for matching the experimentally measured anode current. The fit predicts the entire profile of the electric field, thus lending insight beyond the local electric-field profile in the proximity of the cathode. Other boundary constraints include the 100%-reflection condition at the conical electrode surface and the zero-reflection condition at the other surfaces. The low-energy plasma electrons are assumed to be local and Maxwellian, whereas the energetic electrons are assumed to be nonlocal and non-Maxwellian. Except for these differences, the two populations are described using the same system of time-dependent equations, Eqs. (1)–(4), the steady-state solution of which we present here.

### III. THE MODELING RESULTS AND DISCUSSION

By finding the energetic-electron component of cathode current as a function of primary-anode current for a given voltage between cathode and anode, a comprehensive understanding of the modeled current-voltage characteristics is obtained. Figure 5 shows the modeled current-voltage characteristics of the cathode-anode gap for auxiliary-anode voltage of 48 V and for anode current of 0.2 A (curve A) and 0.4 A (curve B) as well as the respective experimental measurement (dashed line). The level of agreement is sufficient to conclude confidently that the cathode-anode gap has a positive differential resistance and plasma is stable. Additional experimental evidence confirms both that the discharge exhibits neither oscillations nor instabilities for these parameters and that auxiliary-anode current reduction toward zero is accompanied by the differential resistance of the cathode-anode gap transforming from positive to negative and the rise of discharge instability and oscillations.

Typical potential profiles in the cathode-anode gap for the low-voltage discharge are shown in Fig. 6. The cathode fall<sup>15–17</sup> and the potential well for low-energy electrons are depicted in the experimental data and the model. The depth of

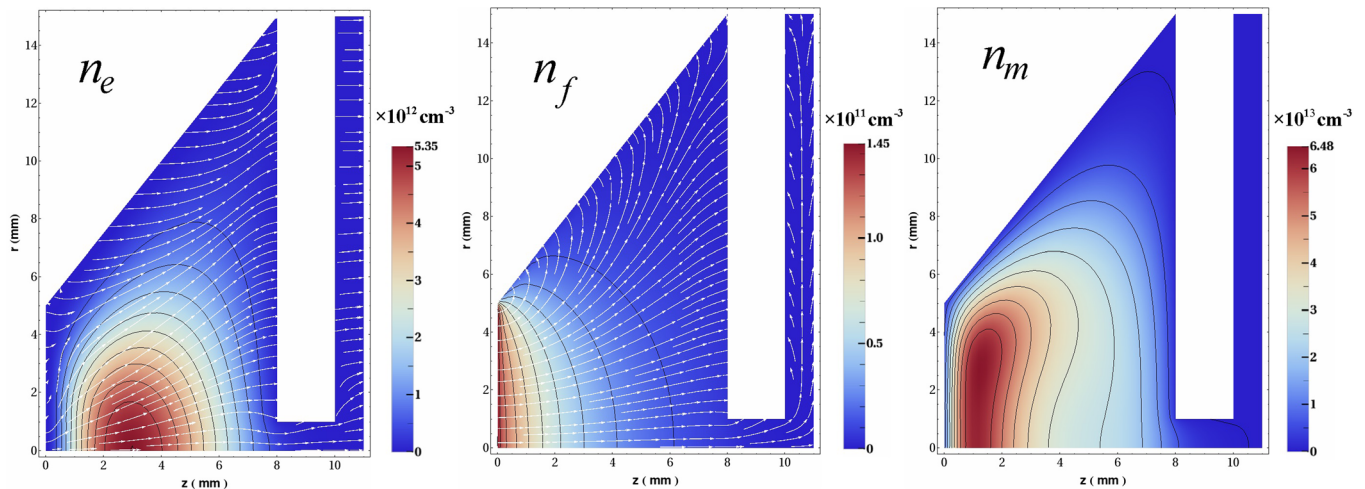


FIG. 7. Density colorplot of low-energy plasma electrons (right), energetic electrons (middle), and metastable atoms (left) for the discharge parameters  $T_e = 2$  eV and  $U_d = 19$  V. Plasma electron and ion fluxes are indicated by arrows.

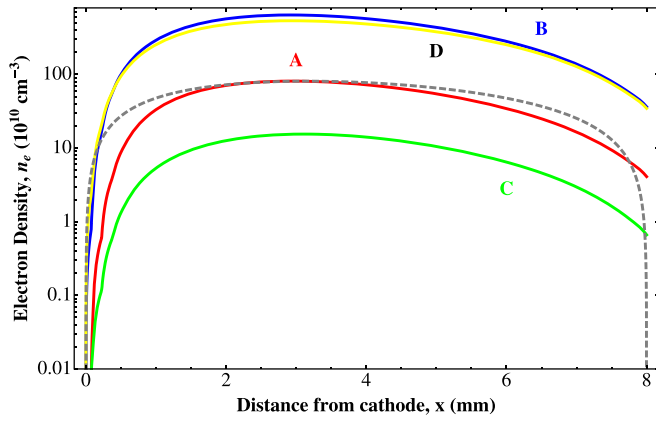


FIG. 8. Axial distribution of the density of slow electrons in the cathode-anode gap. Letters A–D mark profiles corresponding to the same conditions as in Fig. 5. The dotted line is the approximation of the axial profile of the electron (A) (15), with parameter  $\Lambda = 3$  mm.

this well is determined by the ambipolar potential energy drop from Eq. (12) and has a magnitude of a few times the electron thermal energy (see, e.g., Refs. 5 and 17). The narrow space-charge sheath region is characterized by the sheath-potential jump between cathode and plasma that exceeds the voltage applied between the cathode and the anode  $U_d$ .

The agreement between experimental data and the model predictions is sufficient to confirm that, for the discharge conditions studied, the low-energy plasma electrons are electrostatically trapped in the region that comprises the cathode-anode gap. From this confirmation, we expect that, with the auxiliary anode, the low-energy plasma electrons are characterized by a Maxwellian and the energetic

electrons emitted by the cathode are characterized with beam energy slightly above the atomic excitation energy and ionization energy, matching the electron distribution functions in the case without an auxiliary anode. The excitation of the gas atoms is mostly due to energetic electrons, while both energetic and low-energy plasma electrons contribute to the stepwise ionization.

Figure 7 shows the two-dimensional spatial distribution of the low-energy plasma electron density ( $n_e$ ), energetic electrons density ( $n_f$ ), and metastable helium atom density ( $n_m$ ) for the discharge parameters  $T_e = 2$  eV and  $U_d = 19$  V. The spatial distribution of the plasma ion density (not shown here) resembles that of the plasma electrons. It is evident from Fig. 7 that the low-energy plasma electron density smoothly decays to all boundaries in typical diffusive fashion and the plasma ion density profile behaves similarly. In the simplest case, where the total ionization source in Eq. (1) decreases exponentially with the length scale  $\Lambda$ ,  $Z_m = \exp(-x/\Lambda)$ , the solution of the one-dimensional ambipolar diffusion equation<sup>20</sup> is

$$\frac{n(x)}{n_\Lambda} = 1 - e^{-\frac{x}{\Lambda}} - \frac{x}{L} (1 - e^{-\frac{x}{\Lambda}}), \quad (15)$$

where  $n_\lambda = z_m \Lambda^2 / D_a$ . Fig. 8 shows examples of the solution of Eq. (15) as well as the prediction of simulations. The discrepancy near the cathode is attributed to the proximity of the conical wall and to the wall's influence on the loss of the electrons, neither of which is taken into account in Eq. (15).

Metastable atoms have a diffusive-like density profiles also. Fig. 9 shows the predicted axial density profiles of metastable helium atoms for cases A–D of Fig. 6. Note that, typical for this type of discharge,<sup>5</sup> the metastable-atom density

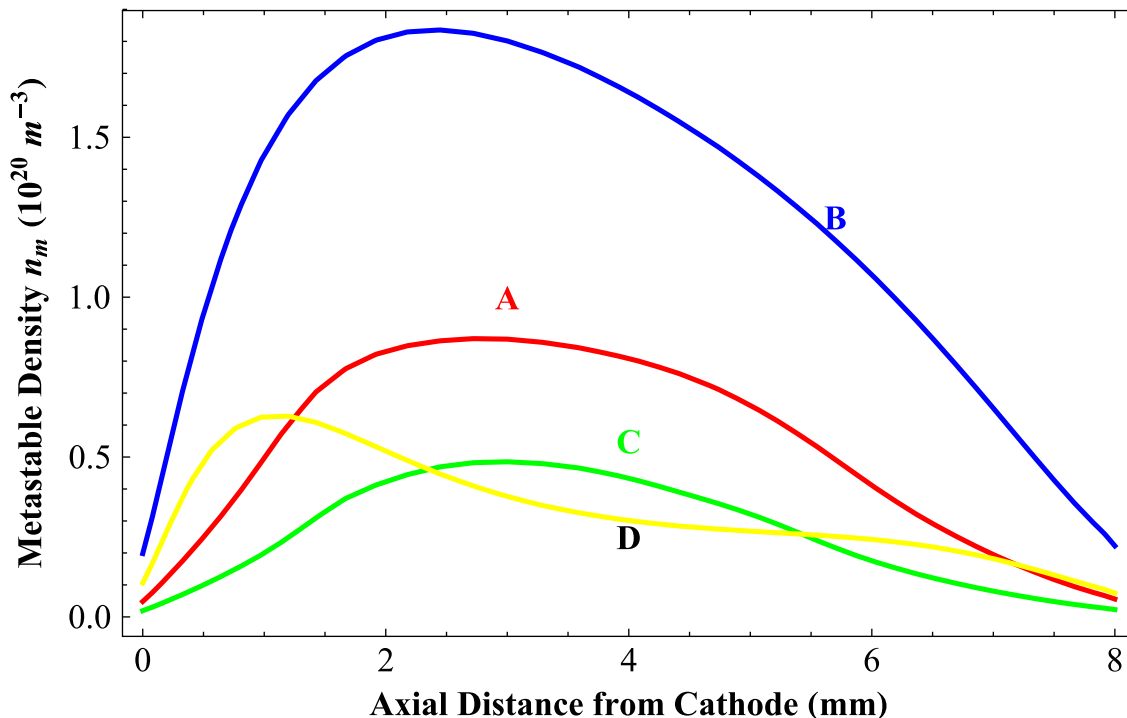


FIG. 9. Axial density profile of metastable helium atoms in the cathode-anode gap. Curves marked A–D correspond to the same conditions as in Fig. 6.

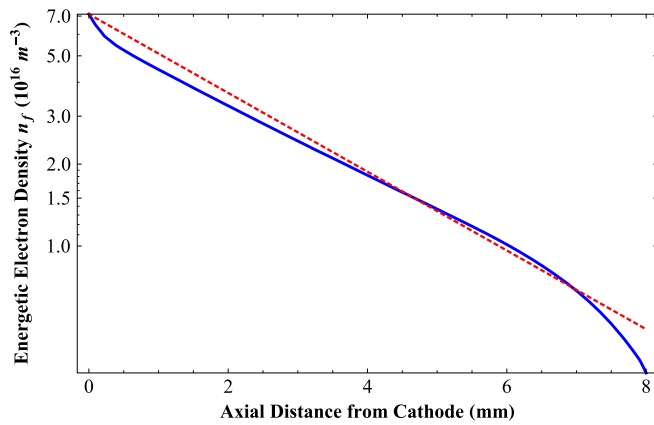


FIG. 10. The simulation's predicted radial profile of energetic electrons for the case having  $T_e = 1$  eV and  $U_d = 15$  V. The dotted line is predicted from Eq. (16) using the exponential decay constant  $c = 3$  mm.

peak can be more than an order of magnitude larger than the low-energy plasma-electron density peak.

The balance of energetic electrons emitted from the cathode is determined by their diffusion to the anode and to the side wall as well as by their energy loss by both inelastic excitation and ionization. Assuming that the density exponentially decreases with distance from the cathode  $x$

$$n_f(x) = n_{f0} \cdot \exp(-x/\Lambda), \quad (16)$$

that the characteristic scale of the decrease can be expressed as

$$\frac{1}{\Lambda} = \frac{1}{\lambda_{\epsilon}^*} + 1/\bar{\Lambda} \quad (17)$$

and that in Eq. (17),  $\lambda_{\epsilon}^* = \sqrt{\lambda\lambda^*}$  is the length of the energy relaxation of energetic electrons,  $\bar{\Lambda} \approx (R_1 + R_2)/2 \times 2.4 \approx 4$  mm is the expression for the average effective radial diffusion length.

Predictions from Eq. (16) are illustrated in Fig. 10, where, for example, the predicted axial profile of the energetic electrons is shown for the regime with  $T_e = 1$  eV and  $U_d = 15$  V. The dotted line shows the dependence of Eq. (16) with an exponential density decay constant  $c = 3$  mm in Eq. (17).

The agreement between the analytical model and the simulation illustrates the profiles of the low-energy plasma electrons and metastable-atoms depend sensitively on the value of potential to which the primary anode is adjusted. The electron density varies by more than an order of magnitude across its axial profile (Fig. 8) and the density of metastable helium atoms varies almost an order of magnitude (Fig. 9) across its axial profile. Adjusting the value of primary-anode potential adjusts the current (Fig. 5) and leads to a temperature change in the low-energy plasma electrons (Fig. 4).

## IV. CONCLUSIONS

The proposed model relates the experimental current-voltage characteristics to the plasma parameters of the short dc discharges having an auxiliary anode beyond the primary anode. The model confirms the explanation of the observation of oscillation-free discharge plasma when current is collected to the auxiliary anode. The model explains the discharge's unstable oscillations in the absence of auxiliary-anode current collection. In the latter case, plasma instability leads to numerical noise in the model and impossibility to obtain stable regime. The model reproduces the sensitivity of the auxiliary-anode current and other plasma parameters to the primary-anode potential and auxiliary-anode potential. Specifically, the model demonstrates the positive differential resistance in the current-voltage relationship of the discharge with two anodes. Therefore, such a discharge should be effective in an engineering application that requires a current and voltage stabilizer

## ACKNOWLEDGMENTS

This research was supported by the DOE Fusion Energy Sciences contract DE-SC0001939, by SPbGU, by ITMO and by AFOSR.

- <sup>1</sup>L. D. Tsendin, *Plasma Sources Sci. Technol.* **4**, 200 (1995).
- <sup>2</sup>L. D. Tsendin, *Plasma Sources Sci. Technol.* **18**, 014020 (2009).
- <sup>3</sup>L. D. Tsendin, *Phys. Usp.* **53**, 133 (2010).
- <sup>4</sup>A. S. Mustafaev, V. I. Demidov, I. Kaganovich, S. F. Adams, M. E. Koepke, and A. Grabovskiy, *Rev. Sci. Instrum.* **83**, 103502 (2012).
- <sup>5</sup>Y. P. Raizer, *Gas Discharge Physics* (Springer, New York, 1997).
- <sup>6</sup>Z. Lj. Petrovic, I. Stefanovic, S. Vrhovac, and J. Zivkovic, *J. Phys. IV* **7**, C4-341 (1997).
- <sup>7</sup>A. V. Phelps *et al.*, *Phys. Rev. E* **47**, 2825 (1993).
- <sup>8</sup>I. Stefanovic *et al.*, *J. Appl. Phys.* **110**, 083310 (2011).
- <sup>9</sup>F. Greiner, T. Klinger, A. Rohde, and A. Piel, *Phys. Plasmas* **2**, 1822 (1995).
- <sup>10</sup>F. Greiner, T. Klinger, and A. Piel, *Phys. Plasmas* **2**, 1810 (1995).
- <sup>11</sup>I. Kaganovich, M. A. Fedotov, and L. D. Tsendin, *Sov. Phys. Tech. Phys.* **39**, 241 (1992).
- <sup>12</sup>V. I. Demidov, C. A. DeJoseph, Jr., and V. Ya. Simonov, *Appl. Phys. Lett.* **91**, 201503 (2007).
- <sup>13</sup>I. V. Schweigert, V. I. Demidov, and I. D. Kaganovich, *Phys. Plasmas* **20**, 101606 (2013).
- <sup>14</sup>R. C. G. Leckey, G. S. Higginson, and K. G. Emeleus, *Nature* **198**, 1187 (1963).
- <sup>15</sup>V. I. Demidov, *Sov. Phys.-Tech. Phys.* **25**, 338 (1980).
- <sup>16</sup>V. I. Demidov, C. A. DeJoseph, Jr., and A. A. Kudryavtsev, *Phys. Rev. Lett.* **95**, 215002 (2005).
- <sup>17</sup>N. B. Kolokolov, A. A. Kudryavtsev, and A. B. Blagoev, *Phys. Scr.* **50**, 371 (1994).
- <sup>18</sup>V. A. Godyak and V. I. Demidov, *J. Phys. D: Appl. Phys.* **44**, 233001 (2011).
- <sup>19</sup>V. I. Demidov, S. V. Ratynskaia, and K. Rypdal, *Rev. Sci. Instrum.* **73**, 3409 (2002).
- <sup>20</sup>E. A. Bogdanov, S. F. Adams, V. I. Demidov, A. A. Kudryavtsev, and J. M. Williamson, *Phys. Plasmas* **17**, 103502 (2010).
- <sup>21</sup>E. A. Bogdanov, K. D. Kapustin, A. A. Kudryavtsev, and A. S. Chirtsov, *Tech. Phys.* **55**, 1430 (2010).